Adsorption 7: 339–356, 2001

Effects of Feed Composition of Coke Oven Gas on a Layered Bed H_2 PSA Process

HYUNGWOONG AHN
Department of Chemical Engineering, Yonsei University, Shinchon-dong, Seodaemun-ku, Seoul 120-749, Korea

JAEYOUNG YANG
R&D Center, SK Engineering & Construction Limited, Kwanhun-dong, Chongro-ku, Seoul 110-300, Korea

CHANG-HA LEE*
Department of Chemical Engineering, Yonsei University, Shinchon-dong, Seodaemun-ku, Seoul 120-749, Korea
leech@yonsei.ac.kr

Received December 11, 2000; Revised August 13, 2001; Accepted September 20, 2001

Abstract. The effects of feed composition on the adsorption dynamics and the optimal process design were studied from the experimental and simulated results in the H_2 layered bed PSA with activated carbon and zeolite 5A. The breakthrough results using the "base composition" (56.4 vol% H_2; 26.6 vol% CH_4; 8.4 vol% CO; 5.5 vol% N_2; and 3.1 vol% CO_2) in various layered beds were compared with those using the "higher nitrogen composition" and the "no nitrogen composition". In the breakthrough dynamics, the propagation velocity of wave front of each component was closely related to the slope of isotherm estimated at its concentration in the feed. Breakthrough behavior at each layered bed in the "higher nitrogen composition" showed similar trends as that in the "base composition". However, the "no nitrogen composition" showed different breakthrough behavior from the other groups. In this feed composition, it was observed that the order of CO and CH_4 breakthrough times was reversed with a change in the carbon-to-zeolite ratio. Based on the adsorption dynamics and breakthrough behavior of each feed composition group in various layered beds, the effect of feed composition on a seven-step two-bed PSA process for the H_2 recovery from coke oven gas was investigated numerically to develop a well-designed H_2 PSA process under various operating conditions. As expected from the breakthrough results, the trends of the PSA performance in the "higher nitrogen composition" were similar to those in the "base composition" except for the slight decrease in the optimal carbon-to-zeolite ratio. However, in case of the "no nitrogen composition", high purity product was obtained from the activated carbon-rich layered bed PSA because the adsorption capacity of the activated carbon for impurities was superior to that of zeolite. As a result, the optimum carbon-to-zeolite ratio at each operating condition was slightly changed depending on the propagation velocity of each component on each layer.

Keywords: 7 step H_2 PSA process, breakthrough, feed composition effect, layered bed

Introduction

Pressure swing adsorption (PSA) has been extensively used in the industry to obtain desired product by separation and purification. Due to the increasing demand of hydrogen for petroleum refinery and petrochemical processing, a strong economic motivation has prompted the development of processes to recover hydrogen from refinery off-gases, coke oven gas (COG), etc. Many versions of the H_2 PSA process

*To whom correspondence should be addressed.

incorporating two to twelve adsorption beds have been developed for 99.99–99.9999% purity hydrogen with 70–90% recovery (Yang, 1987; Ruthven et al., 1994).

In the previous studies (Klein and Vermeulen, 1975; Frey, 1983; Wankat and Tondeur, 1985), a layered bed was applied to a PSA process for the improvement in the efficiency. Some PSA processes using layered beds have been set up at an industrial scale for multicomponent gas separation (Chlendi and Tondeur, 1996; Watson et al., 1996). Also, the adsorption dynamics in the bed and its optimal design were studied from the experimental and simulated breakthroughs in the layered bed composed of the activated carbon and the zeolite 5A for H_2 mixture separation (Park et al., 1998; Yang and Lee, 1998). More recently, the adsorption dynamics of a layered bed and the performance of a layered bed H_2 PSA using COG have been studied (Lee et al., 1999; Ahn et al., 1999). They also pointed out that controlling the wave front of leading component among all impurities played a very important role in obtaining a high purity product in a PSA process.

Since the PSA unit is usually located at the downstream of the total process, the feed composition of the PSA process might vary slightly with time. Kumar (1994) studied the effects of direct feeding of the variable composition feed on the PSA process by numerical simulation. He pointed out that the increasing impurity case performed better and the decreasing impurity case performed worse than the average feed concentration case. However, the feed composition shows no significant variation during a short period of time except in case of providing directly the feed gas from the upstream process to the PSA unit. The most common method to mitigate the effect of these variations is to install a mixing vessel at the upstream of the PSA and design the adsorption system based upon the average feed composition. Therefore, the factor that has conspicuous effect upon the performance of the PSA process is the variation of the average feed composition rather than the temporal variation in the feed composition. In case of coke oven gas stemmed from the steel industries, the change in the feed composition by coke or upstream operating condition cannot be controlled by a mixing vessel. Since this changed composition will be supplied to the PSA unit for a certain period of time, understanding adsorption dynamics is needed to deal with the change in the feed composition.

The adsorption step plays a key step to developing a well-designed H_2 PSA process. In this study, the adsorption dynamics and the breakthrough behavior in layered beds with various activated carbon-to-zeolite ratio were investigated from breakthrough experiments with three different feed composition groups. Since it was nitrogen that proved to be the most important impurity to obtain a high H_2 purity product from COG, the three different average feed composition groups with different amount of nitrogen were used. Based on the breakthrough results, the effects of feed composition on a seven-step layered two-bed PSA process with a backfill step for H_2 recovery from COG was investigated numerically under various operating conditions. The dynamics of breakthrough and H_2 PSA process were analyzed by using a non-isothermal dynamic model incorporating mass, energy and momentum balances. Detailed analysis of the layered bed for various COG feeds can be used to design an optimal layered bed for a H_2 PSA process.

Experimental

The feed composition based on the related literatures (Lee et al., 1999) was defined as a "base composition" (56.4 vol% H_2; 26.6 vol% CH_4; 8.4 vol% CO; 5.5 vol% N_2; and 3.1 vol% CO_2) and the results of this composition were compared with those of two different feed composition groups; One was the "higher nitrogen composition" in which N_2 concentration reached up to 7.5% because this composition was sometimes discharged at steel industry. The other was the "no nitrogen composition", indicating a four-component feed gas mixture with higher CO_2 composition than the other two composition groups. The three different feed composition groups used in this study are shown in Table 1.

Table 1. Feed composition for three cases.

	Feed composition (vol%)				
Case	CH_4	CO	N_2	CO_2	H_2
Base composition	26.6	8.4	5.5	3.1	56.4
Higher nitrogen composition	26.6	8.4	7.5	3.1	54.4
No nitrogen composition	26.6	8.4	0.0	8.6	56.4

Before the experiment, the activated carbon (PCB, Calgon Co., 6–16 mesh) and the zeolite 5A (W. R. Grace Co., 4–8 mesh) were regenerated for more than 12 hours at 323 K and 593 K, respectively. After putting the activated carbon into the bottom of the bed, zeolite 5A was added. Then, the adsorption bed was initially saturated with H_2 at the adsorption pressure.

The schematic diagram of the experimental apparatus is shown in Fig. 1. The adsorption bed was made of stainless steel of 100 cm length and 3.71 cm ID. To measure the temperature inside the bed, four RTDs (Pt 100Ω) were installed at the positions of 10, 30, 50 and 75 cm from the feed end. The pre-calibrated mass flow controller (Bronkhorst High-Tech, F-201C) was installed between a feed tank and adsorption bed to control the feed rate. The total amount of gas was confirmed by a wet gas meter (Shinagawa, W-NK-1B). The electrical back-pressure regulator between the adsorption bed and the product tank was installed to maintain constant adsorption pressure in the bed. Effluent stream was sampled between the back-pressure regulator and the product tank and was analyzed by using a mass spectrometer (Balzers, QME 200). Due to the same main mass spectrum of CO and N_2 in mass spectrometer, the breakthrough curves of these gases were confirmed by GC (HP, GC 5890 II). The characteristics of the adsorption bed and the adsorbents used in the experiment and simulation are shown in Table 2.

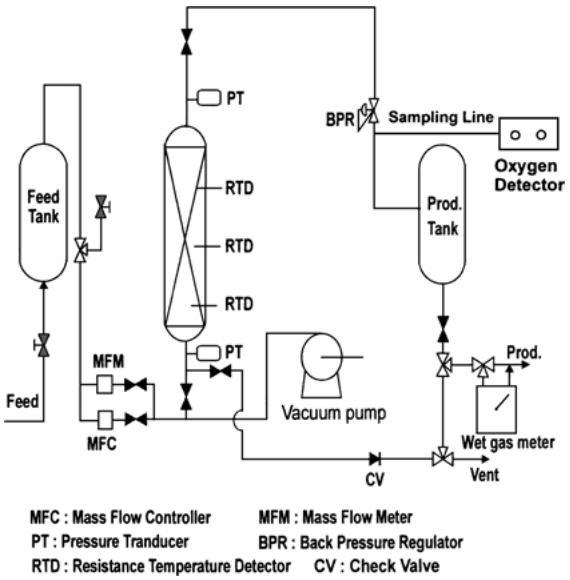

Figure 1. Experimental apparatus for breakthrough experiment.

Table 2. Characteristics of the adsorption bed and adsorbents.

Adsorption bed		
Length		100 cm
Inside diameter		3.71 cm
Outside diameter		4.245 cm
Heat capacity of wall		0.12 cal/g · K
	Activated carbon bed	Zeolite bed
Bulk (bed) density	0.482 g/cm^3	0.764 g/cm^3
External void fraction	0.433	0.357
total void fraction	0.78	0.77
Adsorbents		
	Activated carbon	Zeolite 5A
Pellet size	6–16 mesh	4–8 mesh
Pellet density	0.85 g/cm^3	1.16 g/cm^3
Heat capacity	0.25 cal/g · K	0.22 cal/g · K

Mathematical Model

Using the axially dispersed plug flow and an ideal gas law, the material balance for the bulk phase in the adsorption column was given by

$$-D_L\frac{\partial^2 y_i}{\partial z^2}+\frac{\partial y_i}{\partial t}+u\frac{\partial y_i}{\partial z} + \frac{RT}{P}\frac{1-\varepsilon}{\varepsilon}\rho_p\left(\frac{\partial \bar{q}_i}{\partial t}-y_i\sum_{j=1}^{n}\frac{\partial \bar{q}_j}{\partial t}\right)=0 \quad (1)$$

By applying an ideal gas law to Eq. (1), the overall mass balance could be represented as follows:

$$-D_L\frac{\partial^2 P}{\partial z^2}+\frac{\partial P}{\partial t}+P\frac{\partial u}{\partial z}+u\frac{\partial P}{\partial z} + PT\left(-D_L\frac{\partial^2(1/T)}{\partial z^2}+\frac{\partial(1/T)}{\partial t}+u\frac{\partial(1/T)}{\partial z}\right) -2D_L T\frac{\partial(1/T)}{\partial z}\frac{\partial P}{\partial z}+\frac{1-\varepsilon}{\varepsilon}\rho_p RT\sum_{j=1}^{n}\frac{\partial \overline{q_j}}{\partial t}=0 \quad (2)$$

In Eqs. (1) and (2), the axial dispersion coefficient, D_L, was calculated by a Wakao equation using interstitial feed velocity at the adsorption pressure and this constant value was used for all the steps (Wakao and

Funazkri, 1978):

$$\frac{D_L}{2uR_p} = \frac{20}{\text{Re Sc}} + 0.5 \tag{3}$$

Assuming thermal equilibrium between fluid and particles, the energy balance for gas and solid phases was given by

$$-K_L\frac{\partial^2 T}{\partial z^2} + (\alpha\rho_g(C_p)_g + \rho_B(C_p)_s)\frac{\partial T}{\partial t} + \rho_g(C_p)_g\,\varepsilon u\frac{\partial T}{\partial z} - \rho_B\sum_i^n Q_i\frac{\partial \overline{q_i}}{\partial t} + \frac{2h_i}{R_{B_i}}(T - T_w) = 0 \tag{4}$$

The effective axial thermal conductivity in Eq. (4), K_L, was estimated by the following empirical correlation (Kunii and Smith, 1960; Suzuki, 1990).

$$K_L/k_g = K_{L0}/k_g + 6\text{Pr Re} \tag{5a}$$

$$K_{L0}/k_g = \varepsilon + \frac{1-\varepsilon}{\phi + (2/3)(k_g/k_s)} \tag{5b}$$

$$\phi = \phi_2 + (\phi_1 - \phi_2)\left(\frac{\varepsilon - 0.26}{0.216}\right) \quad \text{for } 0.260 \le \varepsilon \le 0.476 \tag{5c}$$

The constant effective axial thermal conductivity, which was estimated by using Eq. (5) under the experimental condition of the adsorption step, was used for the simulation of that run.

Due to the small diameter of the bed, another energy balance for the wall of the adsorption bed was used:

$$\rho_w(C_p)_w A_w\frac{\partial T_w}{\partial t} = 2\pi R_{Bi}h_i(T - T_w) - 2\pi R_{Bo}h_o(T_w - T_{atm}) \tag{6a}$$

$$A_w = \pi\left(R_{Bo}^2 - R_{Bi}^2\right) \tag{6b}$$

The Ergun's equation shown below was applied to the pressure drop across the bed (Alpay et al., 1993; Kikknides and Yang, 1993; Lu et al., 1993; Yang et al., 1998).

$$-\frac{dP}{dz} = a\mu v + b\rho v|v| \tag{7a}$$

$$a = \frac{150}{4R_p^2}\frac{(1-\varepsilon)^2}{\varepsilon^3}, \quad b = 1.75\frac{(1-\varepsilon)}{2R_p\varepsilon^3} \tag{7b}$$

where v is superficial velocity.

The sorption rate into the adsorbent pellet was described by the following linear driving force (LDF) model, with a single lumped mass transfer parameter, ω (Yang, 1987; Ruthven et al., 1994).

$$\frac{\partial \overline{q_i}}{\partial t} = \omega_i(q_i^* - \overline{q_i}) \tag{8}$$

The equilibrium of mixture was described by the following extended Langmuir-Freundlich model:

$$q_i = \frac{q_{mi}B_iP_i^{n_i}}{1 + \sum_{j=1}^n B_jP_j^{n_i}} \tag{9a}$$

$$q_m = k_1 + k_2T, \quad B = k_3e^{k_4/T}, \quad n = k_5 + k_6/T \tag{9b}$$

Then, the slope of isotherm at a partial pressure of adsorbate can be calculated by the following differential form from the extended Langmuir-Freundlich model in Eq. (9a).

$$\left.\frac{\partial q_i}{\partial P_i}\right|_{\substack{p_i \\ p_j = const.(j\neq i,\ j=1,2,\ldots,N)}} = \left.\frac{q_{mi}B_in_iP_i^{n_i-1}\left(1 + \sum_{j=1\,j\neq i}^N B_jP_j^{n_j}\right)}{\left(1 + \sum_{j=1}^n B_jP_j^{n_j}\right)^2}\right|_{\substack{p_i \\ p_j = const.(j\neq i,\ j=1,2,\ldots,N)}} \tag{9c}$$

The well-known Danckwerts boundary conditions were applied to the steps that have influent streams. Since the bed was initially saturated with H_2 up to the adsorption pressure, only the boundary condition for the adsorption step in a PSA process was applied to the breakthrough simulation. Also, the input parameters for the L-F model and LDF model as well as the boundary conditions used in the PSA simulation were described at the previous works in detail (Ahn et al., 1999; Jee et al., 2001).

Process Cycle and Conditions for PSA Simulation

In order to obtain an H_2 product with a desired level of high purity and recovery from various sources containing many kinds of impurity, industrial H_2 PSA processes were generally operated using a backfill step and layered beds simultaneously (Lee et al., 1999; Ahn

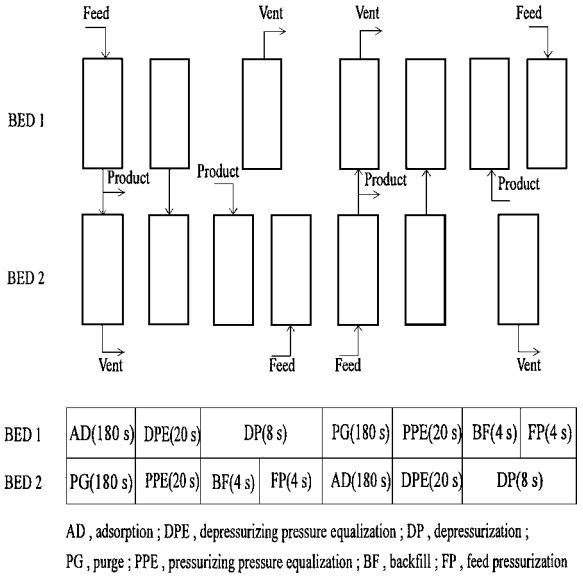

Figure 2. Flow diagram and cycle sequence of a seven-step two-bed PSA process.

et al., 1999). In this study, H_2 PSA process in the simulation consisted of two adsorption beds and each bed was operated by the following cyclic sequence: (1) feed pressurization of a partially pressurized bed by a previous pressurizing pressure equalization step and a backfill step (FP), (2) high-pressure adsorption (AD), (3) depressurizing pressure equalization (DPE), (4) countercurrent depressurization (DP), (5) purge with a light product, H_2 (PG), (6) pressurizing pressure equalization (PPE), (7) backfill step with a light product up to the average of the AD pressure and the PPE pressure (BF). The cyclic sequence for this seven-step process with step times and a simple flow diagram were illustrated in Fig. 2. The carbon-to-zeolite ratio (c.r.) was defined as a ratio of the activated carbon layer length to bed length (Yang and Lee, 1998). The PSA processes with various carbon-to-zeolite ratios were simulated in the range of 6 to 11 LSTP/min feed rate (5.55 m/s to 10.2 m/s in superficial gas velocity), 6 to 12 atm adsorption pressure and 0.3 to 1.0 LSTP/min purge rate (0.278 m/s to 0.925 m/s in superficial gas velocity).

Results and Discussion

Effects of Feed Composition and Carbon-to-Zeolite Ratio on Breakthrough Curves

Adsorption equilibrium for every pure component on activated carbon and zeolite 5A was measured by a volumetric method at several temperatures (283.15 K, 293.15 K, and 303.15 K). The measured pure gas adsorption isotherms on activated carbon and zeolite 5A at 293.15 K are shown in Fig. 3.

The propagation velocity of the concentration wave front of each component depends on its isotherm because the curvature of the isotherm at a given pressure indicates the intensity of interaction force between the adsorbent and adsorbate at that pressure (Yang, 1987). The propagation velocity of each component can be calculated by the following equation.

$$u_{c_i} = \left(\frac{\partial z}{\partial t}\right)_{c_i} = \frac{u}{1 + \frac{1-\varepsilon}{\varepsilon}\frac{\Delta q_i}{\Delta c_i}\Big|_{c_i}} \tag{10}$$

In case of a favorable isotherm, the propagation velocity of the adsorbate with high concentration is faster than that with its low concentration, which causes a compressive or self-sharpening wave front. In case of an unfavorable type, however, the propagation velocity shows the reverse phenomenon due to the dispersive wave front. In this study, all the isotherms of the impurities showed favorable types in both activated carbon and zeolite 5A. Therefore, as the concentration of the adsorbate in the bed became higher, its propagation velocity of the adsorbate became faster at that condition. Also, the adsorption dynamics in the layered bed can be explained by using Eq. (10).

The experimental breakthrough curves using three different feed composition groups were presented in Figs. 4–6. In order to investigate the effect of the carbon-to-zeolite ratio on the feed composition, breakthrough experiments were performed at three different layered beds.

Figure 4 shows the experimental breakthrough curves of three different hydrogen mixtures in the layered bed with 0.32 c.r. under 9.68 atm adsorption pressure and 8.6 LSTP/min feed rate. As shown in this figure, the simulated results agreed well with the experimental results. As shown in Fig. 4(a) representing the breakthrough of the "base composition," the H_2 PSA performance in respect of product purity is expected to depend strongly on its ability to remove N_2. In the zeolite-rich layered bed with 0.32 c.r., the role of zeolite 5A layer on the adsorption dynamics was more dominant than that of activated carbon layer. In the zeolite 5A layer under the partial pressure of each component, the $\Delta q_i/\Delta c_i$ in CO isotherm was greater than that of CH_4 isotherm by about 1.2 times. Therefore,

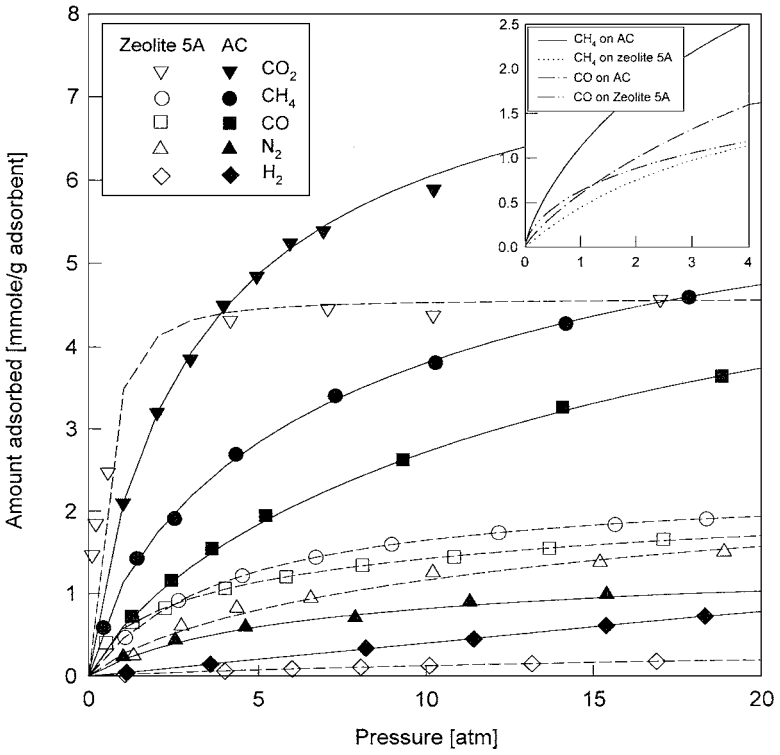

Figure 3. Adsorption isotherms of CO_2, CH_4, CO, N_2, and H_2 on zeolite 5A and activated carbon at 293.15 K.

the propagation velocity of CH_4 mass transfer zone (MTZ) in Eq. (10) approached the product end faster than that of CO MTZ.

In order to study the effect of nitrogen which is a crucial factor in separation performance, the breakthroughs of "higher nitrogen composition" and "no nitrogen composition" in Fig. 4(b) and (c) were compared with that of "base composition" at the same layered bed. In the breakthrough of the "higher nitrogen composition", the breakthrough time of N_2 was faster by about 54 sec than that of the "base composition" under the same operating conditions due to the increased propagation velocity of N_2 MTZ. Except for the early breakthrough and the higher roll-up of N_2, the behavior of breakthrough curves in this composition was similar to that of the "base composition".

In case of the "no nitrogen composition" in Fig. 4(c), however, the breakthrough time of H_2 was elongated and showed a sharp breakthrough curve. Meanwhile, contrary to the other composition groups, CO_2 was detected in the effluent stream early due to the higher concentration of CO_2 in the feed. Also, it is noted that the roll-up in the CH_4 breakthrough curve was observed twice. After the first small roll-up in the front part of the CH_4 breakthrough curve by the CO MTZ, the second broad roll-up was caused by CO_2 MTZ.

In Fig. 5, the carbon-to-zeolite ratio in the configuration of adsorption bed was changed from 0.32 in Fig. 4 to 0.5 under the same operating conditions. Compared with Fig. 4, the breakthrough time of H_2 in all the feed composition groups were elongated. Also, in Fig. 5(a) and (b), the difference between the breakthrough time of N_2 and that of other impurities in this bed became greater than their difference in Fig. 4. Moreover, the breakthrough time of CH_4 was almost the same as that of CO as shown in Fig. 5. This is because the $\Delta q_i / \Delta c_i$ in CH_4 isotherm was greater by about 1.2 times than that in CO isotherm in the activated carbon layer under the partial pressure condition of each component, which is different from the zeolite 5A layer. Therefore, in the layered bed with 0.5 c.r., the difference in the propagation velocities of CO and CH_4 in the activated carbon layer was almost offset by that in the zeolite layer. Moreover, in case of the "no nitrogen composition" in Fig. 5(c), the small but clear roll-up of CO was observed, which was not shown in the zeolite-rich bed.

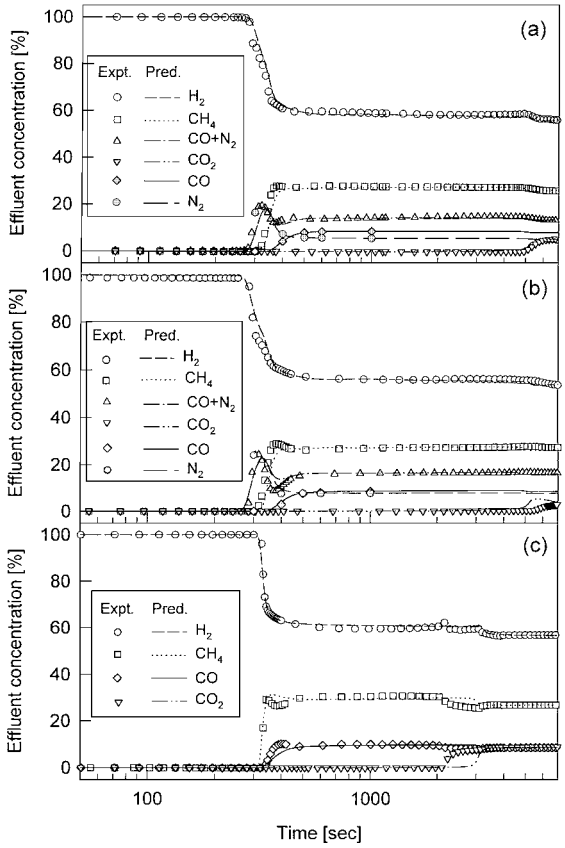

Figure 4. Breakthrough curves of (a) "base composition" (Jee et al., 2001), (b) "higher nitrogen composition", and (c) "no nitrogen composition" in the layered bed with the 0.32 carbon-to-zeolite ratio under the 10 atm adsorption pressure and 8.6 LSTP/min feed rate.

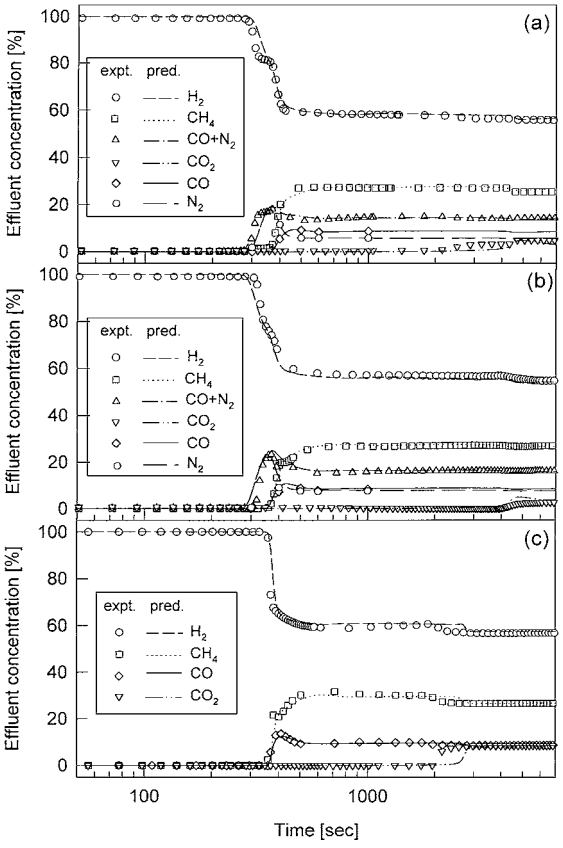

Figure 5. Breakthrough curves of (a) "base composition" (Jee et al., 2001), (b) "higher nitrogen composition", and (c) "no nitrogen composition" in the layered bed with the 0.5 carbon-to-zeolite ratio under the 10 atm adsorption pressure and 8.6 LSTP/min feed rate.

Figure 6 shows the breakthrough results of three composition groups in the activated carbon-rich bed with 0.65 c.r. Compared with the breakthrough results at the zeolite-rich bed in Fig. 4, the reversion in the breakthrough order of CO and CH_4 was observed. The breakthrough time of CH_4 in the layered bed with 0.65 c.r. became slightly slower than that of CO. Since the activated carbon layer was elongated, the concentration wave front of CH_4 in the activated carbon-rich bed propagated more slowly than those in any other layered bed. Therefore, the small roll-up of CO was observed in Fig. 6(a) and (b). Also, since the zeolite layer was shortened, the breakthrough of N_2 in Fig. 6(a) and (b) was faster than those in any other bed. Especially, the sharp roll-up of CO by CH_4 and the broad roll-up of CH_4 by CO_2 were shown in Fig. 6(c). Also, the breakthrough time of CO_2 in the activated carbon-rich bed was shorter than those in any other beds.

As shown in these results, the breakthrough behavior of each component was affected by the feed composition and the carbon-to-zeolite ratio of a layered bed. Especially, the concentration change of strong adsorbate (CO_2) in the feed gave a detrimental effect on the breakthrough behavior of other components, while the concentration change of weak adsorbate (N_2) affected just the breakthrough time of itself. Also, the propagation velocity of the concentration wave front of each component on each adsorbent depended on its isotherm.

Breakthrough Dynamics in the Layered Beds

To gain a clearer insight into the adsorption dynamics of each feed composition in various layered beds, concentration profiles in the gas phase at 180 sec

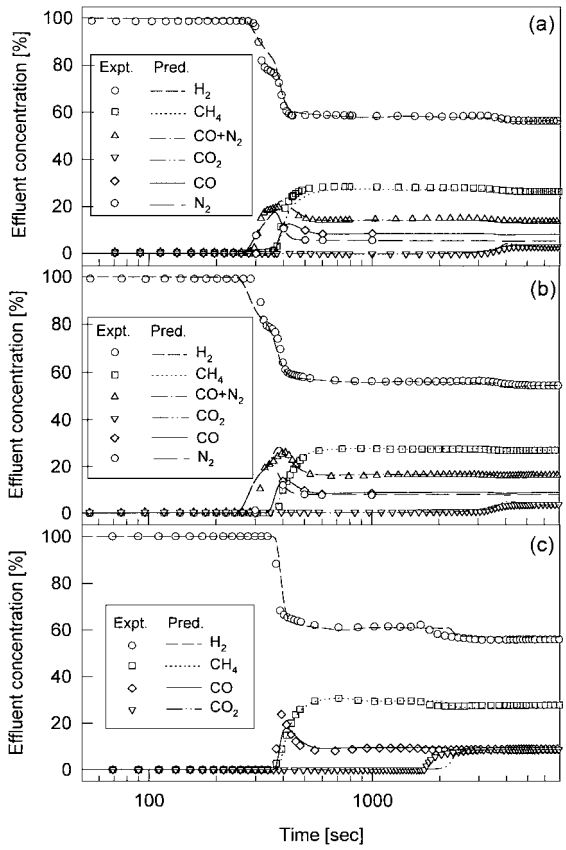

Figure 6. Breakthrough curves of (a) "base composition" (Jee et al., 2001), (b) "higher nitrogen composition", and (c) "no nitrogen composition" in the layered bed with the 0.65 carbon-to-zeolite ratio under the 10 atm adsorption pressure and 8.6 LSTP/min feed rate.

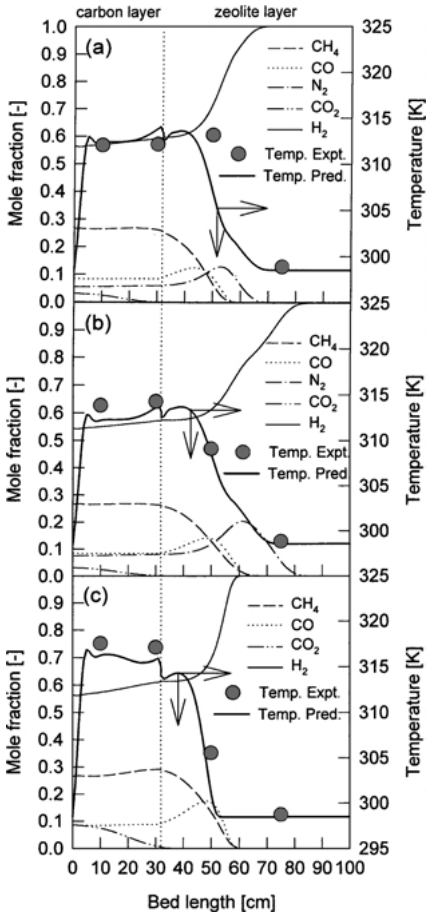

Figure 7. Concentration and temperature profiles in the gas phase at the 180 sec in the breakthrough simulations of (a) "base composition" (Jee et al., 2001), (b) "higher nitrogen composition", and (c) "no nitrogen composition" in the layered bed with the 0.32 carbon-to-zeolite ratio under the 10 atm adsorption pressure and 8.6 LSTP/min feed rate.

from the beginning of the step input are presented in Figs. 7 to 9 with temperature profiles. Furthermore, these results help predict the dynamic behavior of a PSA process with 180 sec adsorption step time in this study.

Figure 7 shows the concentration profile and the temperature excursion in a layered bed with 0.32 c.r. in Fig. 4. In all of these three composition groups, CH_4 MTZ caught up with CO MTZ. Therefore, it is expected that CH_4 MTZ would reach the product end before CO MTZ as shown in Fig. 4. The MTZ of CO component progressed to the product end further than that of CH_4 in the activated carbon layer because the $\Delta q_i / \Delta c_i$ in CO isotherm was smaller than that in CH_4 isotherm at each partial pressure condition. However, after passing the layer interface, the MTZs of CO and CH_4 became close in the zeolite 5A layer and the slope of H_2 MTZ became very steep. Also, since the difference of the affinities of CO and CH_4 was smaller in the zeolite 5A layer than in the activated carbon layer, the extent of the roll up of CO by CH_4 was small at 180 sec.

The effect of N_2 concentration on the breakthrough time was conspicuous as shown in Fig. 7(a)–(c). In case of the "higher nitrogen composition" in Fig. 7(b), the N_2 MTZ approached the product end further than that in case of the "base composition" in Fig. 7(a). Even though the concentrations of CO and CH_4 in the feed were the same as those in the "base composition", these concentration profiles advanced to the product end further than those in the "base composition". Because of the favorable type of N_2 isotherm, the N_2 MTZ proceeded along the bed at a higher velocity than that in case of the "base composition".

Therefore, if the mole fraction of the component which propagated faster than any other wave fronts was increased, that component will affect product purity directly and much more attention should be paid to the PSA process design or the set-up of the operating condition.

In the "no nitrogen composition" in Fig. 7(c), it is interesting that the wave fronts of CO and CH_4 MTZs propagated almost the same as those in Fig. 7(a) but the temperature profile was different from that in Fig. 7(a). Increased CO_2 concentration in the feed led to increased roll-ups and steep concentration wave fronts of CH_4 and CO. Therefore, at this position, the front of the temperature profile decreased steeply and the H_2 MTZ became steep. However, since the concentration wave front of CO_2 at this time passed through a layer interface, it might have a detrimental effect on the regeneration of a zeolite layer in the PSA process.

In Fig. 8, the carbon-to-zeolite ratio in the layered bed was increased from 0.32 to 0.5. While the MTZs of all the components except CO_2 transgressed the layer interface in Fig. 7, the CH_4 MTZ and most of the CO MTZ at 180 sec breakthrough time in all of the three composition groups remained in the activated carbon layer in Fig. 8. Contrary to the 0.32 c.r. bed, the CH_4 and CO MTZs were clearly separated due to the dominating effect of the activated carbon layer. Also, because the adsorption capacity of CH_4 was greater than that of CO in the activated carbon layer, the extent of the roll-up of CO by CH_4 was great in comparison to that in the 0.32 c.r. bed. Therefore, the concentration profile of H_2 in all composition groups underwent a stepwise change as shown in Fig. 4. The concentration wave front of N_2 proceeded to the product end more than that in 0.32 c.r. bed in Fig. 7 due to the shortened zeolite layer. Therefore, as shown in Fig. 8(a) and (b), small temperature excursion at the layer interface was observed in the "base composition" and "higher nitrogen composition" due to mainly the adsorption of N_2. However, since the MTZs of impurities except N_2 were located away from the product end rather than those in the 0.32 c.r. layered bed, the PSA process with this 0.5 c.r. bed is expected to make a product with improved purity. Meanwhile, since the wide separation among the MTZs of impurities leads to a broad concentration profile of H_2 over the bed, it will give a detrimental effect on the product recovery in the PSA process. However, in case of the "no nitrogen composition", the concentration wave fronts and roll-ups of CO and CH_4 in Fig. 8(c) became steeper and propagated more slowly than those in Fig. 7(c) due to the increased activated carbon layer. Also, the temperature profile showed a steep decrease around the layer interface. Therefore, it can be expected that the H_2 purity in the "no nitrogen composition" can be improved by an increase in the carbon-to-zeolite ratio.

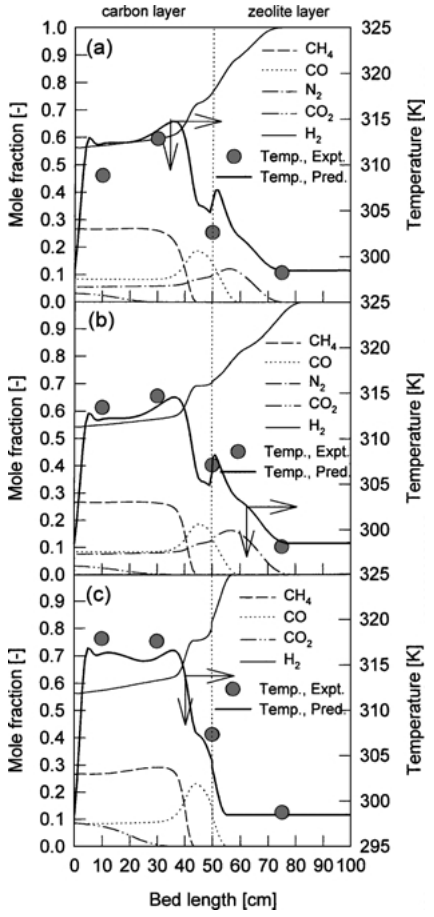

Figure 8. Concentration and temperature profiles in the gas phase at the 180 sec in the breakthrough simulations of (a) "base composition" (Jee et al., 2001), (b) "higher nitrogen composition", and (c) "no nitrogen composition" in the layered bed with the 0.5 carbon-to-zeolite ratio under the 10 atm adsorption pressure and 8.6 LSTP/min feed rate.

As shown in Fig. 9, impurities except N_2 were held in the activated carbon layer at 0.65 c.r. bed and all MTZs were clearly separated. As a result, the concentration profile of H_2 showed a stepwise change clearly similar to the results in Fig. 8. In Fig. 9(a) and (b), however, the N_2 MTZ proceeded further to the product end than in the 0.5 c.r. layered bed due to the shortened zeolite length. Also, because of the different adsorption heat of

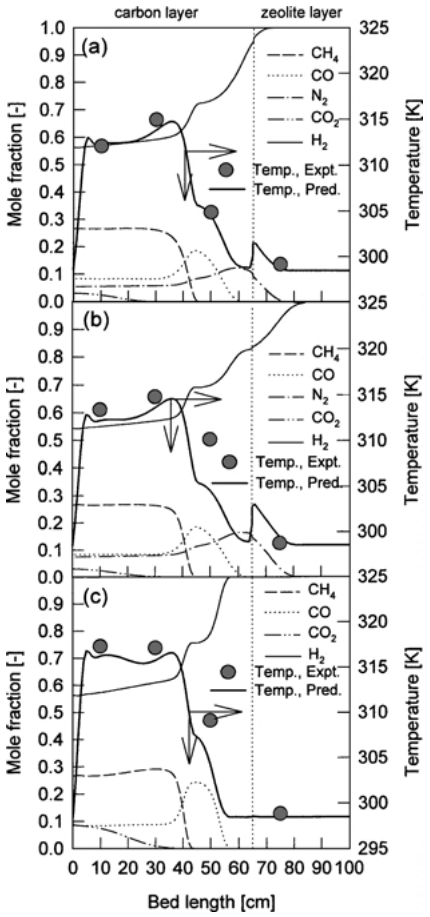

Figure 9. Concentration and temperature profiles in the gas phase at the 180 sec in the breakthrough simulations of (a) "base composition" (Jee et al., 2001), (b) "higher nitrogen composition", and (c) "no nitrogen composition" in the layered bed with the 0.65 carbon-to-zeolite ratio under the 10 atm adsorption pressure and 8.6 LSTP/min feed rate.

N_2 between activated carbon and zeolite, the temperature excursion took place at the layer interface. In case of the "no nitrogen composition" in Fig. 9(c), the concentration wave fronts of all impurities at 180 sec were held in the activated carbon layer and the MTZ velocity of CO was slightly faster than in the 0.5 c.r. layered bed. Since most CO was adsorbed in the activated carbon layer, zeolite layer was suitable for removing the trace amount of CO in order to obtain a high purity product as shown in Fig. 8(c). As a result, since zeolite 5A has greater adsorption capacity for N_2 as well as very low concentration range of CO than activated carbon, the zeolite layer could work as a purifier for CO and N_2 in the mixture treated bulkily by the activated carbon layer.

Effects of Feed Composition on the Layered Bed H_2 PSA

Based on the breakthrough results, the effects of feed composition on a seven-step layered two-bed H_2 PSA process with a backfill step was investigated numerically to obtain an optimum operating condition. The change in purity and recovery with carbon-to-zeolite ratio at each composition group was discussed under various operating conditions such as feed rate, adsorption pressure and purge rate.

Effects of Feed Rate and Carbon-to-Zeolite Ratio. Figure 10 shows the effects of feed rate and carbon-to-zeolite ratio on the simulated PSA process using

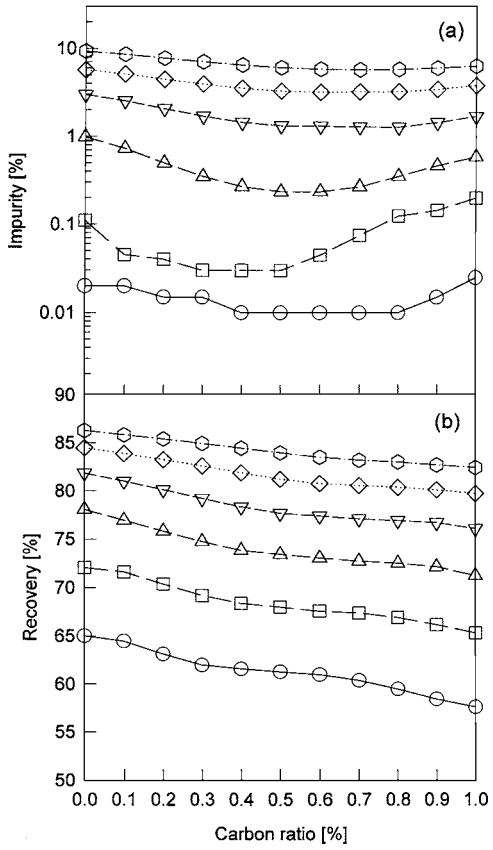

Figure 10. Effects of feed rate and carbon-to-zeolite ratio on (a) product purity and (b) recovery of the simulated PSA process using the "base composition" as a feed under 10 atm adsorption pressure and 0.7 LSTP/min purge rate. (—○—, 6 LSTP/min; —□—, 7 LSTP/min; —△—, 8 LSTP/min; —▽—, 9 LSTP/min; ···◇···, 10 LSTP/min; —○—, 11 LSTP/min).

the "base composition" as a feed under the condition of 10 atm adsorption pressure and 0.7 LSTP/min purge rate. The simulation was done in a range of 6 LSTP/min to 11 LSTP/min feed rate with an interval of 1 LSTP/min.

As shown in Fig. 10(a), the amount of product impurity with carbon-to-zeolite ratio at the same operating condition showed a concave shape. In order to obtain the highest purity from each condition, the carbon-to-zeolite ratio moved from about 0.7 to 0.5 as the feed rate decreased. At the high feed rate over 8 LSTP/min, the MTZs of impurities moved further to the product end in the adsorption step. Therefore, the length of the activated carbon layer in the bed should be elongated for bulk separation because the adsorption capacity of the activated carbon for most impurities such as CO_2, CH_4 and CO was superior to that of zeolite. However, at less than 7 LSTP/min feed rate, the best product purity could be obtained in the layered bed process with 0.5 c.r. Moreover, a higher than 99.99+% H_2 purity could be obtained only in a layered bed PSA process at the 6 LSTP/min feed rate.

Since the concentration profiles in the zeolite 5A bed was the steepest in all kinds of beds at the blowdown step (Ahn et al., 1999), the loss of H_2 could be minimized at this bed. Therefore, at the same product purity condition, the recovery in the zeolite-rich bed process was higher than that in the activated carbon-rich bed process as shown in Fig. 10(b). Also, even though the product amount increased in proportion to feed rate, the net amount of H_2 in the product did not increase linearly because the loss of H_2 at the blowdown step increased with a decrease in the feed rate.

Figure 11 shows the simulated results representing the effects of feed rate and carbon-to-zeolite ratio on the PSA performance using the "higher nitrogen composition" under the same operating conditions in Fig. 10. In Fig. 11(a), while the PSA performance was similar to that of the "base composition", the carbon-to-zeolite ratio giving the highest purity moved from around 0.6 to 0.4 with a decrease in the feed rate. However, under the same operating condition, the highest H_2 purity value in this composition group was lower than that in the "base composition". It implied the importance of N_2 amount in the feed because it became a leading wave front in the adsorption bed.

As mentioned in the breakthrough experiments, another important thing was that the optimum carbon-to-zeolite ratio for purity moved to a slightly lower value than that in the "base composition" due to the weak

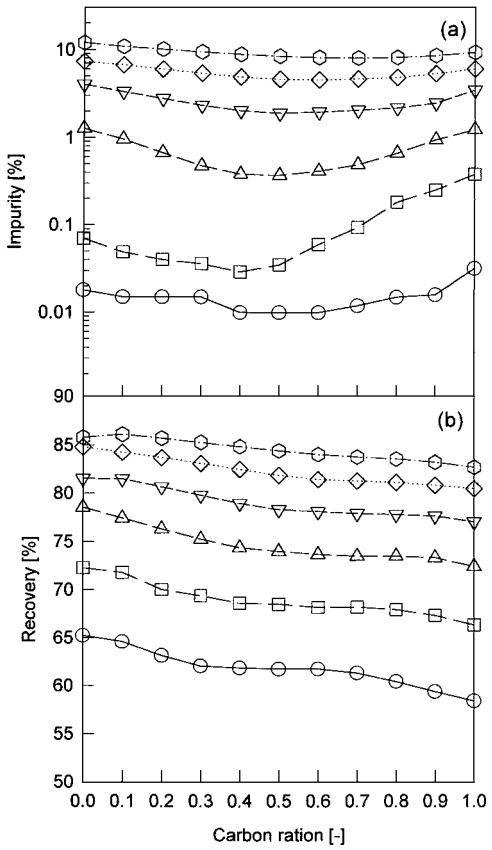

Figure 11. Effects of feed rate and carbon-to-zeolite ratio on (a) product purity and (b) recovery of the simulated PSA process using the "higher nitrogen composition" as a feed under 10 atm adsorption pressure and 0.7 LSTP/min purge rate. (—○—, 6 LSTP/min; —□—, 7 LSTP/min; —△—, 8 LSTP/min; —▽—, 9 LSTP/min; ···◇···, 10 LSTP/min; —⊙—, 11 LSTP/min).

adsorption capacity of the activated carbon for N_2. Especially, the product purity in the activated carbon-rich bed process became worse than that in the "base composition". This phenomenon implied that with the increase of N_2 in the feed composition, the zeolite layer played a more important role in a removal of N_2. Also, the non-linearlity of recovery with carbon-to-zeolite ratio was slightly greater than that in the "base composition" as shown in Fig. 11(b).

Figure 12 shows the effects of feed rate and carbon-to-zeolite ratio on the PSA performance using the "no nitrogen composition". In this composition as shown in Table 1, N_2 was not present in the feed and CO_2 composition was increased from 3.1% to 8.6%. In case of the "no nitrogen composition", since the adsorption capacity of the activated carbon for impurities was superior to that of zeolite 5A, the PSA process using only

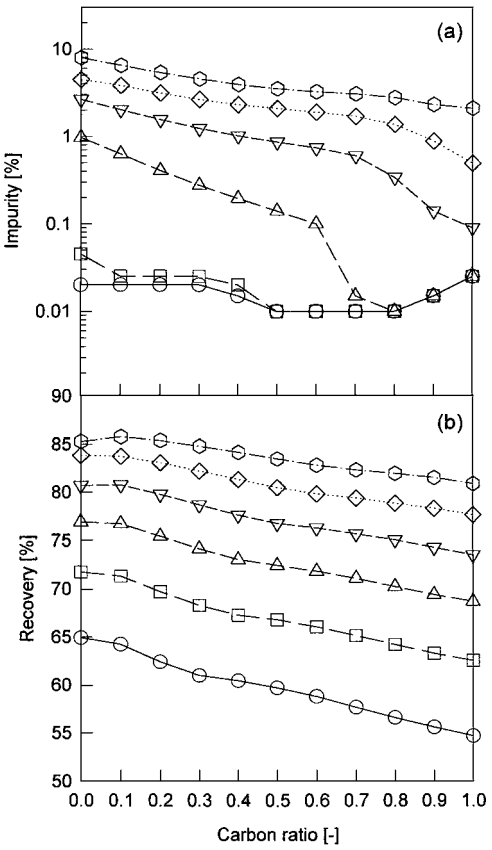

Figure 12. Effects of feed rate and carbon-to-zeolite ratio on (a) product purity and (b) recovery of the simulated PSA process using the "no nitrogen composition" as a feed under 10 atm adsorption pressure and 0.7 LSTP/min purge rate. (—○—, 6 LSTP/min; —□—, 7 LSTP/min; —△—, 8 LSTP/min; —▽—, 9 LSTP/min; ···◇···, 10 LSTP/min; —⬡—, 11 LSTP/min).

activated carbon could give the best purity under the high feed rate conditions. Since a lot of impurities had to be removed at the high feed rate, the zeolite 5A layer could not work well as a purifier of CO and only the activated carbon layer became important as a bulk separator. Especially, due to the increased amount of CO_2 in the feed, the zeolite 5A bed process would accompany a significant swing of temperature by strong adsorption. This was very unfavorable in a PSA process because higher temperature reduced adsorption capacity in the adsorption step and lower temperature in the desorption step made desorption more difficult. Therefore, the improvement of product purity with a decrease in the feed rate was observed in activated carbon-rich bed processes as the feed rate changed from 9 to 8 LSTP/min. Meanwhile, as the feed rate changed from 8 LSTP/min to 7 LSTP/min, the effect of feed rate on purity was more significant in the zeolite-rich bed processes than in the activated carbon-rich bed processes. This is because the activated carbon layer in the zeolite-rich bed can hold the concentration wave front of CO_2 as mentioned in the breakthrough section.

In Fig. 12, when the activated carbon bed was used, product purity reached 99.5% even at 10 LSTP/min feed rate. However, to obtain a 99.99% purity product, the carbon-to-zeolite ratio moved to the activated carbon-rich layered bed process from the activated carbon bed process with a decrease in feed rate. This was because the zeolite 5A layer was superior to the activated carbon layer in purifying the trace amount of CO. In addition, the effect of carbon-to-zeolite ratio on product purity was very significant at the same operating condition, compared with other feed cases in Figs. 10 and 11. Moreover, a high purity product with 99.99+% was obtained from the activated carbon-rich bed process in the "no nitrogen composition" at higher feed rate condition compared to the other feed composition cases. Since the impurities are remained in the activated carbon layer as shown in Fig. 9, the short length of the zeolite 5A layer with 0.8 c.r. is enough to purify a small amount of CO. Moreover, the difference in recovery between 8 LSTP/min and 6 LSTP/min at this bed process was more than 10% even at the same product purity because the bed was used inefficiently at low feed rate. Therefore, at constant product purity, the recovery in the activated carbon-rich bed process is higher than that in the zeolite-rich bed process. Also, a decrease in the recovery with an increase in the carbon-to-zeolite ratio was slightly steeper than that in the "base composition".

Effects of Adsorption Pressure and Carbon-to-Zeolite Ratio. Figure 13 shows the simulated results representing the effects of carbon-to-zeolite ratio and adsorption pressure on the simulated PSA process using the "base composition" under the condition of 7 LSTP/min feed rate and 0.7 LSTP/min purge rate. Purity and recovery were simulated from 6 to 12 atm adsorption pressure with an increase of 1 atm. The increase in adsorption pressure prevented all the impurities from proceeding to the product end, similar to the effect of the decrease in feed rate. Accordingly, as shown in Fig. 13(a), the optimum carbon-to-zeolite ratio for the best purity at each condition moved from 0.5 to 0.4 as the pressure increased from 6 atm to 10 atm. However, the optimum carbon-to-zeolite ratio over 11 atm moved again from 0.4 to 0.5. This was

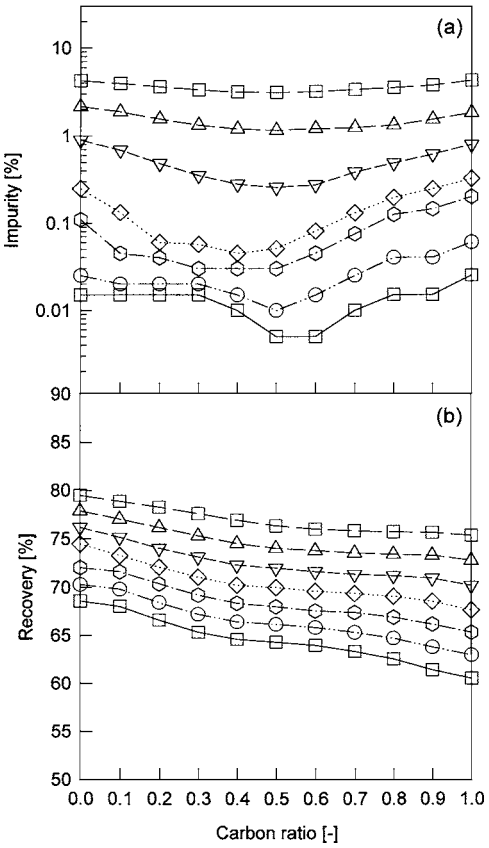

Figure 13. Effects of adsorption pressure and carbon-to-zeolite ratio on (a) product purity and (b) recovery of the simulated PSA process using the "base composition" as a feed under 7 LSTP/min feed rate and 0.7 LSTP/min purge rate. (⊟, 6 atm; △, 7 atm; ▽, 8 atm; ◇, 9 atm; ○, 10 atm; ⊙, 11 atm; ⊟, 12 atm).

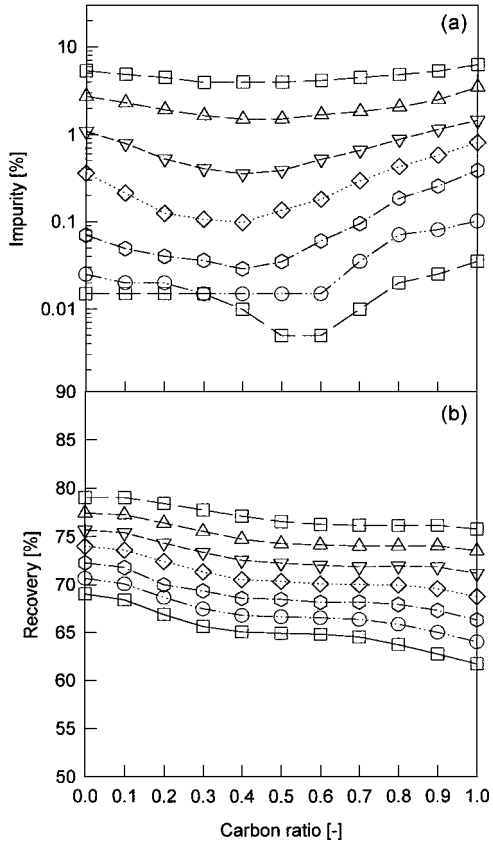

Figure 14. Effects of adsorption pressure and cabon-to-zeolite ratio on (a) product purity and (b) recovery of the simulated PSA process using the "higher nitrogen composition" as a feed under 7 LSTP/min feed rate and 0.7 LSTP/min purge rate. (⊟, 6 atm; △, 7 atm; ▽, 8 atm; ◇, 9 atm; ○, 10 atm; ⊙, 11 atm; ⊟, 12 atm).

because the increase in the adsorption capacity with pressure was more significant in the activated carbon layer than in the zeolite layer around this pressure.

Unlike the effects of feed rate, H_2 recovery dropped almost linearly with the adsorption pressure for all types of the adsorption bed in Fig. 13(b). This was because the amount of H_2 loss from the feed end during a countercurrent depressurization step was proportional to the adsorption pressure or, more accurately speaking, to the pressure of the pressure equalization step. Therefore, at the same product purity with 99.99% H_2, the 0.5 c.r. bed process at 11 atm gave higher recovery than the 0.4 c.r. and 0.7 c.r. bed processes at 12 atm. As a result, the optimum carbon-to-zeolite ratio can improve purity as well as recovery at constant product purity.

In Fig. 14(a) and (b), the purity and recovery in the "higher nitrogen composition" case under the same operating conditions showed a similar trend as those in the "base composition" case, showing that the purity and recovery in the "higher nitrogen composition" were slightly lower than those in the "base composition". However, as the pressure was increased, the carbon- to-zeolite ratio to obtain best purity from each operating condition moved quickly from 0.5 to 0.4 compared with the results in the "base composition" case. This was because the longer zeolite layer is needed to treat the increased N_2 in this feed composition than that in the "base composition" case as mentioned in the breakthrough results.

In case of the "no nitrogen composition" as shown in Fig. 15, the PSA process using only activated carbon gave best purity at a low adsorption pressure range like the result of the effect of feed rate. From the 8 atm adsorption pressure, the importance of the zeolite 5A

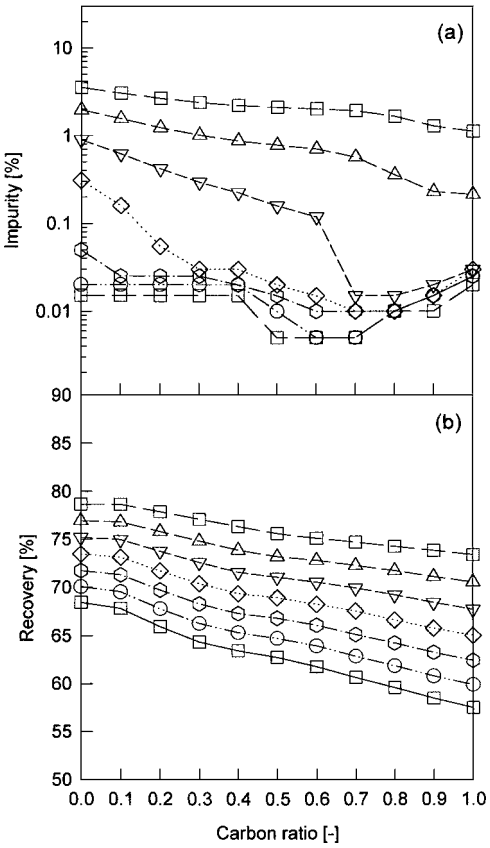

Figure 15. Effects of adsorption pressure and carbon-to-zeolite ratio on (a) product purity and (b) recovery of the simulated PSA process using the "no nitrogen composition" as a feed under 7 LSTP/min feed rate and 0.7 LSTP/min purge rate. (⊟, 6 atm; △, 7 atm; ▽, 8 atm; ◇, 9 atm; ⊖, 10 atm; ⊙, 11 atm; ⊟, 12 atm).

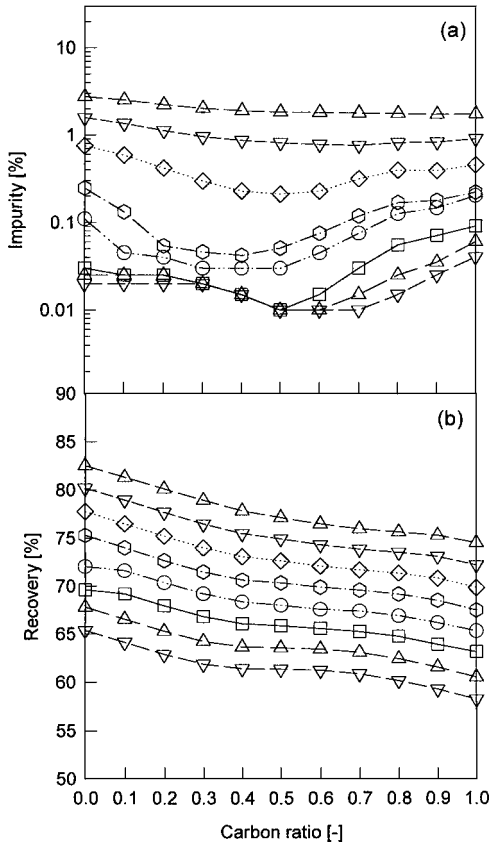

Figure 16. Effects of purge rate and carbon-to-zeolite ratio on (a) product purity and (b) recovery of the simulated PSA process using the "base composition" as a feed under 7 LSTP/min feed rate and 10 atm adsorption pressure. (△, 0.3 LSTP/min; ▽, 0.4 LSTP/min; ◇, 0.5 LSTP/min; ⊖, 0.6 LSTP/min; ⊙, 0.7 LSTP/min; ⊟, 0.8 LSTP/min; △, 0.9 LSTP/min; ▽, 1.0 LSTP/min).

layer as a purifier of CO showed up and, therefore, the PSA process giving the best product purity moved from the activated carbon bed process to the activated carbon-rich bed process. Moreover, in order to obtain the high purity product with 99.99+% H_2, the carbon-to-zeolite ratio decreased up to 0.6 to purify trace amount of CO by strong adsorption in the zeolite layer. Also, similar to the results in the effect of feed rate, a decrease in the recovery with an increase in the carbon-to- zeolite ratio was slightly steeper than that in the "base composition" case as shown in Fig. 15(b).

Effects of Purge Rate and Carbon-to-Zeolite Ratio. Figure 16 shows the effect of carbon-to-zeolite ratio and purge rate from 0.3 to 1.0 LSTP/min on the simulated PSA process using the "base composition" as feed stream under 10 atm adsorption pressure and 7 LSTP/min feed rate. As shown in Fig. 16(a), in the range of low purge rate, the effect of purge rate on purity was more conspicuous in the zeolite-rich bed process than in the activated carbon-rich bed process. However, the optimum ratio for purity at above 0.8 LSTP/min purge rate changed again to 0.5. Especially, while the purge rate at above 0.8 LSTP/min hardly affected product purity in the zeolite-rich bed process, the activated carbon-rich bed process was still affected by the purge rate in this range. The activated carbon bed at the purge step can easily be regenerated because of the relatively weak adsorption of these impurities on the surface, while the zeolite 5A bed at that step still maintained widely dispersed concentration fronts (Ahn et al., 1999). Therefore, the purge rate at above 0.8 LSTP/min could not have any effects on the

zeolite-rich process any more, while all the wave concentration fronts spread continuously out to the feed end in the activated carbon-rich bed process with an increase in the purge rate.

For recovery in Fig. 16(b), the zeolite 5A bed process was better than any other bed processes at the same operating condition. Based on the same product purity in the range of a high purity product, the recovery in the zeolite-rich bed process was higher than that in the activated carbon-rich bed process. However, the zeolite 5A bed process did not approach the desired product purity (99.99+%) even with an increase in the purge rate.

In Fig. 17, the purity at the same operating condition in the "higher nitrogen composition" was slightly lower than that in the "base composition" and, therefore, the recovery in the "higher nitrogen composition" was also worse than that in the "base composition". Since the zeolite 5A layer was affected by the purge rate more than the activated carbon layer at the low purge rate, the optimum carbon-to-zeolite ratio decreased up to 0.4 with an increase in the purge rate. Also, similar to the "base composition", the optimum carbon-to-zeolite rate must be increased with a high purge rate over 0.8 LSTP/min. However, unlike the "base composition", it showed the optimum value around 0.4 carbon-to-zeolite ratio in case of the 0.8 LSTP/min due to increased N_2 in the feed.

In case of the "no nitrogen composition" as shown in Fig. 18, like the results of the effects of feed rate and adsorption pressure, the activated carbon bed process

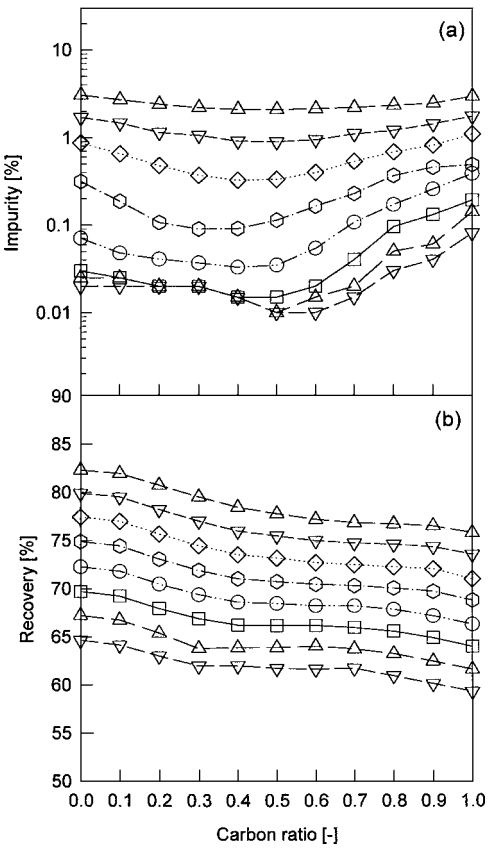

Figure 17. Effects of purge rate and carbon-to-zeolite ratio on (a) product purity and (b) recovery of the simulated PSA process using the "higher nitrogen composition" as a feed under 7 LSTP/min feed rate and 10 atm adsorption pressure. (–△–, 0.3 LSTP/min; –▽–, 0.4 LSTP/min; ···◇···, 0.5 LSTP/min; –○–, 0.6 LSTP/min; –⊙–, 0.7 LSTP/min; –□–, 0.8 LSTP/min; –△–, 0.9 LSTP/min; –▽–, 1.0 LSTP/min).

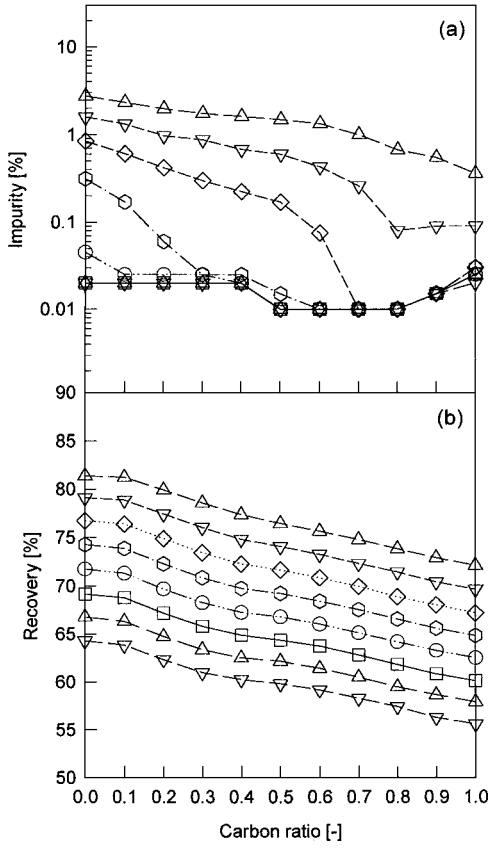

Figure 18. Effects of purge rate and carbon-to-zeolite ratio on (a) product purity and (b) recovery of the simulated PSA process using the "no nitrogen composition" as a feed under 7 LSTP/min feed rate and 10 atm adsorption pressure. (–△–, 0.3 LSTP/min; –▽–, 0.4 LSTP/min; ···◇···, 0.5 LSTP/min; –○–, 0.6 LSTP/min; –⊙–, 0.7 LSTP/min; –□–, 0.8 LSTP/min; –△–, 0.9 LSTP/min; –▽–, 1.0 LSTP/min).

Table 3. Carbon-to-zeolite ratio and operating conditions for maximum recovery with 99.99+% H_2 purity in a seven-step PSA process.

	Carbon-to-zeolite ratio (−)	Adsorption pressure (atm)	Feed rate (LSTP/min)	Purge rate (LSTP/min)
High nitrogen composition	0.5	12	6	0.9
Base composition	0.5	11	6	0.8
No nitrogen composition	0.8	9	8	0.5

gave best purity at a low purge rate range. The recovery in this composition showed a similar trend as the results of the effect of the adsorption pressure. However, the activated carbon-rich layered bed process gave higher purity than the activated carbon bed process from 0.5 LSTP/min purge rate. Moreover, compared with the other two composition groups, the purge rate at above 5 LSTP/min hardly affected purity in the activated carbon-rich bed process because there is no nitrogen concentration front in the bed.

To sum up, Table 3 represents the operating conditions and carbon-to-zeolite ratio to obtain 99.99% H_2 purity with a maximum recovery from each feed composition group. In the case of the "higher nitrogen composition," the desired purity can be obtained by a small increase in the purge rate and adsorption pressure of the "base composition" under the same bed system. However, in the case of the "no nitrogen composition," the desired purity is easily obtained from the same operating condition with the "base composition" because the optimum operating condition in Table 3 is more favorable than that for the "base composition." However, to obtain the maximum recovery from this composition, the carbon-to-zeolite ratio should be changed from 0.5 to 0.8 even though it is not practical in the industrial field.

Conclusions

The breakthrough dynamics of three composition groups of COG in layered beds with various carbon-to-zeolite ratios were studied experimentally and theoretically. Based on the breakthrough study, a seven-step two-layered bed PSA process for H_2 recovery from COG was investigated numerically for understanding the effects of feed composition and operating variables on the PSA performance.

In the breakthrough experiments, the N_2 component, which was the key impurity leading the wave front, was discharged earlier in the "higher nitrogen composition" than in the "base composition" under the same operating conditions. Moreover, the breakthrough order of CH_4 and CO in the "no nitrogen composition" was determined according to the equilibrium isotherm on activated carbon and zeolite at their partial pressure in the feed. As a result, in view of equilibrium relation on the adsorbent of each component, the length ratio of the activated carbon layer for bulk separation to the zeolite layer for purification should be determined to obtain a high purity and recovery.

In case of the "base composition", the carbon-to-zeolite ratio for 99.99+% purity H_2 product was around 0.5 at various operating conditions. However, if high purity H_2 was not required, a zeolite-rich bed PSA process was better than other processes due to higher H_2 recovery at the same operating condition and the constant purity condition. The dynamics of the "higher nitrogen composition" in the bed were similar to those of the "base composition". In this composition, the optimum carbon-to-zeolite ratio had to be slightly lower than that in the "base composition" because the length of zeolite 5A layer should be elongated for the treatment of the increased N_2 in the feed. Also, the product purity in this case was lower than that in the "base composition" under the same operating condition because N_2 became a leading wave front in both composition cases. In case of the "no nitrogen composition", the wave fronts of impurities in the activated carbon bed were much further away from the product end than in any other beds because the activated carbon layer was more favorable to the bulk separation of all the impurities than the zeolite 5A layer. Therefore, the activated carbon bed under the operating conditions for low H_2 purity product gave best purity compared with any other bed processes. However, the carbon-to-zeolite ratio to obtain 99.99+% H_2 product shifted from the activated carbon bed process to the activated carbon-rich layered bed process.

Based on the 99.9+% H_2 purity product, the recovery of the zeolite-rich bed process in the "base

composition" and "higher nitrogen composition" was higher than that of the activated carbon-rich bed process. However, in case of the "no nitrogen composition", the recovery difference between the zeolite-rich bed process and activated carbon-rich bed process became small. Even though the zeolite 5A bed process could give the highest recovery, high purity H_2 (99.99+%) could not be obtained from a zeolite 5A bed PSA in the range of the three operating variables examined in this study. Moreover, at higher than 99.99+% H_2 purity product from COG, the layered bed PSA proved to be better than the single-adsorbent bed processes in respect to H_2 recovery because the recovery to obtain that purity should be lost more in the zeolite bed process than in the layered bed process.

Nomenclature

a, b	Paramenters in Eq. (7a)
A	Cross sectional area, m^2
B	Langmuir-Freundlich isotherm parameter, atm^{-1}
C_p	Heat capacity, J/kg · K
D_L	Mass axial dispersion coefficient, m^2/s
h	Heat transfer coefficient, $J/m^2 \cdot s \cdot K$
K_L	Effective axial thermal conductivity, J/m · s · K
k_g	Thermal conductivity of fluid, J/m · s · K
k_s	Thermal conductivity of particle, J/m · s · K
n	Langmuir-Freundlich isotherm parameter
P	Pressure, atm
Pr	Prandtl number, $(C_p)_g \mu / k_g$
q_m	Langmuir-Freundlich isotherm parameter, mol/kg
$\bar{q}$	Volume-averaged adsorbed phase concentration, mol/kg
q^*	Equilibrium adsorbed phase concentration, mol/kg
Q	Average isosteric heat of adsorption, J/mol
R	Radius, m
Re	Reynolds number, $\rho_g \nu (2R_p)/\mu$
Sc	Schumidt number, $\mu \rho_g / D_m$
t	Time, s
T	Solid phase and gas phase temperature, K
T_{atm}	Ambient temperature, K
t_s	Stoichiometric breakthrough time, s
u	Interstitial velocity, m/s
y	Mole fraction in gas phase
z	Axial position in a adsorption bed, m

Greek Letters

α	Total void fraction
δ, ϕ	Parameters used in Eq. (5)
ε	Interparticle void fraction
μ	Viscosity, m/kg · s
ν	Superficial velocity, m/s
ρ	Density, m^3/kg
ω	LDF coefficient, s^{-1}

Subscripts

B	Bed
i	Component i
p	Pellet
g	Gas phase
s	Solid phase
w	Wall

Acknowledgment

The financial assistance and support of BK21 and SK Engineering & Construction, Ltd. is gratefully acknowledged.

References

Ahn, H., J. Yang, B. Seo, K. Baek, and C.-H. Lee, "Backfill Cycle of a Layered Bed H_2 PSA Processes," *Adsorption*, **5**, 419–433 (1999).

Alpay, E., C.N. Kenney, and D.M. Scott, "Simulation of Rapid Pressure Swing Adsorption and Reaction Processes," *Chem. Eng. Sci.*, **48**, 3173–3186 (1993).

Chen, A.D., J.A. Ritter, and R.T. Yang, "Nonideal Adsorption from Multicomponent Gas Mixtures at Elevated Pressure on a 5A Molecular Sieves," *Chem. Eng. Sci.*, **45**, 2877– 2894 (1990).

Chlendi, M. and D. Tondeur, "Dynamics of Two-Adsorbent Beds with Flow-Reversal for Gas Separation" in *Fundam. of Adsorption*, M.D. Levan (Ed.), pp. 187–194, Kluwer Academic Publishers, Boston, 1996.

Chlendi, M., D. Tondeur, and F. Rolland, "A Method to Obtain a Compact Representation of Process Performances from a Numerical Simulator: Example of Pressure Swing Adsorption for Pure Hydrogen Production," *Gas. Sep. Purif.*, **9**, 125–135 (1995).

Frey, D.D., "A Model of Adsorbent Behavior Applied to the use of Layered Beds in Cycling Zone Adsorption," *Sep. Sci. Technol.*, **17**, 1485 (1983).

Gray, P.G. and D.D. Do, "Dynamics of Carbon Dioxide Sorption on Activated-Carbon Particles," *AIChE J.*, **37**, 1027–1034 (1991).

Jee, J.-G., M.-B. Kim, and C.-H. Lee, "Adsorption Characteristics of Hydrogen Mixtures in a Layered Bed: Binary, Ternary, and 5-Component Mixtures," *Ind. Eng. Chem. Res.*, **40**, 868–878 (2001).

Kikkinides, E.S. and R.T. Yang, "Effects of Bed Pressure Drop on Isothermal and Adiabatic Adsorber Dynamics," *Chem. Eng. Sci.*, **48**, 1545–1555 (1993).

Kim, W.-G., J. Yang, S. Han, C. Cho, C.-H. Lee, and H. Lee, "Experimental and Theoretical Study on H_2/CO_2 Separation by a Five Step One-column PSA Process," *Korean J. Chem. Eng.*, **12**, 503–511 (1995).

Klein, G. and T. Vermeulen, "Cyclic Performance of Layered Beds for Binary Ion Exchange," *AIChE Symp. Ser.*, **71**(152), 69–76 (1975).

Kumar, R., "Pressure Swing Adsorption Process: Performance Optimum and Adsorbent Selection," *Ind. Eng. Chem. Res.*, **33**, 1600–1605 (1994).

Kunni, D. and J.M. Smith, "Heat Transfer Characteristics of Porous Rocks," *AIChE J.*, **6**, 71 (1960).

Lee, C.-H., J. Yang, and H. Ahn, "Effects of Carbon-to-Zeolite Ratio on Layered Bed H_2 PSA for Coke Oven Gas," *AIChE J.*, **45**, 535–545 (1999).

Lu, Z.P., J.M. Loureiro, A.E. Rodrigues, and M.D. LeVan, "Pressurization and Blowdown of Adsorption Beds—II. Effect of the Momentum and Equilibrium Relations on Isothermal Operations," *Chem. Eng. Sci.*, **48**, 1699–1707 (1993).

Park, J.-H., J.-N. Kim, S.-H. Cho, J.-N. Kim, and R.T. Yang, "Adsorber Dynamics and Optimal Design of Layered Beds for Multicomponent Gas Adsorption," *Chem. Eng. Sci.*, **53**, 3951–3963 (1998).

Ritter, J.A. and R.T. Yang, "Equilibrium Adsorption of Multicomponent Gas Mixtures at Elevated Pressures," *Ind. Eng. Chem. Res.*, **26**, 1679–1686 (1987).

Ruthven, D.M., S. Farooq, and K.S. Knaebel, *Pressure Swing Adsorption*, pp. 165–264, VCH Publishers, New York, 1994.

Suzuki, M., *Adsorption Engineering*, pp. 187–203, Elsevier, Amsterdam, 1990.

Wakao, N. and T. Funazkri, "Effect of Fluid Dispersion Coefficients on Particle-to-Fluid Mass Transfer Coefficients in Packed Beds," *Chem. Eng. Sci.*, **33**, 1375–1384 (1978).

Wankat, P.C. and D. Tondeur, "Use of Multiple Sorbents in Pressure Swing Adsorption, Parametric Pumping and Cycling Zone Adsorption," *AIChE. Symp. Ser.*, **81**(242), 74 (1985).

Watson, C.F., R.D. Whitley, and M.I. Meyer, "Multiple Zeolite Adsorbent Layers in Oxygen Separation," U.S. Patent 5,529,610, 1996.

Yang, J. and C.-H. Lee, "Adsorption Dynamics of a Layered Bed PSA for H_2 Recovery from Coke Oven Gas," *AIChE J.*, **44**, 1325–1334 (1998).

Yang, J., J.-W. Chang, and C.-H. Lee, "Separations of Hydrogen Mixtures by a Two-Bed Pressure Swing Adsorption Process Using Zeolite 5A," *Ind. Eng. Chem. Res.*, **36**, 2789–2798 (1997).

Yang, J., M.-W. Park, J.-W. Chang, S.-M. Ko, and C.-H. Lee, "Effects of Pressure Drop in a PSA Process," *Korean J. Chem. Eng.*, **15**, 211–216 (1998).

Yang, R.T., *Gas Separation by Adsorption Processes*, pp. 1–8, pp. 126–200, Butterworths, Boston, 1987.